

CTU Journal of Innovation and Sustainable Development



ISSN **2588-1418** | e-ISSN **2815-6412**

DOI:10.22144/ctujoisd.2025.064

Elastic modulus of reinforced concrete from bending test

John Ayibatunimibofa TrustGod, Robert Bennett Ataria*, and Charles Kennedy Department of Civil Engineering, Niger Delta University, Nigeria *Corresponding author (robertataria@yahoo.com)

Article info.

Received 25 Sep 2024 Revised 23 Nov 2024 Accepted 31 May 2025

Keywords

Deflection, elastic, modulus, inertial, reinforcement, concrete, transformed section

ABSTRACT

This study demonstrates an experimental approach for direct measurement of RC elastic modulus. This work considered the transformed moment of inertia as an input variable. The planned laboratory study involves subjecting reinforced concrete beams with varying reinforcement ratios from 0.43% to 1.77% and grades of concrete (M7.5, M10, M15, M20) to bending tests. Two equations for elastic modulus determination were developed based on beam theory. The first crack load and the corresponding deflection were measured from the load-deflection curve. The uncracked transformed moment of inertia $(I_{un,tr})$, cracking moment (M_{cr}) , and deflection (∂) at first crack were computed. By substituting the M_{cr} , ∂ and Iun, tr into the deflection equation based on the test setup, the elastic modulus (E) of RC was determined. Results showed that as the concrete grade increases, so does its modulus of elasticity, and it demonstrated a direct correlation between the increase in concrete grade and its modulus of elasticity. It was also observed that as the percentage of reinforcement increases, the elastic modulus of RC increases due to increased flexural stiffness. The derived equations were able to accurately compute the elastic modulus capturing the composite behavior of concrete and reinforcement.

1. INTRODUCTION

Concrete has lately come to be understood as a three-phase composite material (Yang, 1988; Alsalman et al., 2019). The effect of the young modulus of concrete (Ec) of three-phase concrete is considerably affected by the volume percentage of each phase, namely the aggregate-phase, interfacial transition zone (ITZ), and cement paste (Chu et al., 2022), Ec is largely affected by the elastic property of coarse aggregate (James & James, 2012). The Yang (1988) study has given a thorough evaluation of both experimental and theoretical studies regarding the relevance of elastic modulus in concrete. Experimental findings indicate that an increase in the volume fraction of ITZ in concrete results in a reduction in its effective elastic modulus (Peter & Shuaib, 2000; Yang et al., 2021). The

determination of the ITZ volume fraction is influenced by the aggregate surface area, which, in turn, is affected by factors such as gradation, maximum aggregate size, ITZ volume fraction, and other relevant parameters. According to qualitative valuations, the effective elastic modulus showed an increment as a result of an increase in the aggregate sizes (Christensen & Lo, 2002), and densely graded concrete exhibits a higher elastic modulus (Richard, 2002). The modulus of elasticity, a vital material property, is markedly affected by the inherent properties of coarse aggregate, revealing the essential role that aggregate nature plays in defining structural performance (Aïtcinand, 1990; Baalbaki et al., 1991; Gutierrez & Canovas, 1995).

The elastic modulus holds significant importance as a material property, affecting material strains under applied load and consequently influencing structural displacement (Krystian & Stefania, 2015). Engineers require this parameter for simulations of structural behaviour. In concrete, Young's modulus correlates with compressive strength, connecting with the advancement of cement hydration. Therefore, monitoring this parameter (elastic modulus) is crucial.

The engineering significance of the elastic modulus in both reinforcement and concrete cannot be overstated, particularly in assessing the dynamic and static performances of emerging concrete elements (Krystian & Stefania, 2015). This essential parameter is indispensable for deformations, which is crucial to concrete design, as emphasized by Jin and Li (2003). Additionally, it is applicable to existing structures, aiding estimating the level of deterioration. demonstrated by Yazdi et al. (2013) and Lee et al. (2015). The Young modulus can be determined through experimental measurements or estimated considering equations outlined in different codes, particularly for normal-strength concrete. These codes formulate a relationship between the compressive strength and elastic modulus. It is worth noting that the incorporation of rebar minimally affects the bending strength of reinforced concrete, as indicated by Bhargava et al. (2006) and Bae et al. (2016). Designing a reinforced concrete structural element requires a foundational grasp of reinforced concrete buildings, essential material properties, and familiarity with key concepts related to performance principles of design in concrete structures (kulkarni et al., 2014). The objective is to create a structure that satisfies three conditions: safety concerning stability, structural integrity, and strength; satisfactory cost-effectiveness; serviceability in connection with deformation, durability, and stiffness. The examination of the section's behavior under different loading levels involves two aspects: the initial uncracked period and the ultimate collapse condition (Nakin et al., 2018).

During the initial phase of loading on a simply supported beam, where the applied load gradually increases, the moment develop at any given point remains below the moment that causes crack, and the tensile stress exhibit in the concrete remains below its tensile strength as reported by Lee et al. (2015). This phase, known as the uncracked phase, utilizes the whole section effectively to resist the moment. According to Abdullah et al. (2023), the uncracked phase gets to its maximum limit when the

design applied stress equals cracking stress. Once the applied moment increases beyond cracking stress, the ultimate concrete tensile stress exceeds its tensile strength, leading to crack propagation, primarily at the tensile side of the beam (Yazdi et al., 2013). As the load continues to increase, these cracks widen and extend to the neutral axis. Consequently, the effectiveness of the structural element diminishes. With additional increases in the applied stress, the strain in the reinforcement rises, causing the neutral axis to move upward from the original position, which in turn escalates curvature until eventual collapse occurs.

When a beam is made up of two materials subjected to static loading, the different elastic moduli (E values) of the materials lead to a different stress distribution due to varying stiffness and stress resistance capacities. However, when analyzing such a steel-concrete beam, it's feasible to apply elastic-beam theory by theoretically transforming it into either an all-concrete beam or all-internal reinforcement beam, with the first being the more prevalent choice (James & Macgregor, 2012). This transformation involves replacing the steel portion with an equivalent area of concrete with equal axial stiffness (AE). Since the modular ratio (n) represents the ratio of the elastic modulus of reinforcement (Es) to that of concrete (Ec), the resulting concrete area is obtained by multiplying the modular ratio by the area of reinforcement (nAs). Before the occurrence of flexural cracks, the internal reinforcements do displace concrete, which could resist stresses; the transformed internal reinforcement area becomes (n-1) As for both tension and compression reinforcements. The transformed reinforcement area is believed to be located at the same position in the beam element as the original reinforcement area provided (Choi et al., 2002).

In the determination of member forces, particularly for complex structures like indeterminate ones, understanding the geometric and elastic properties crucial. EN1992-1:(2004) very The recommendations provide accurate elastic moduli for reinforcement and concrete independently; nevertheless, reinforced concrete (RC), contains both steel and concrete. However, in software-based analyses for multi-storey buildings, the focus is often on the sectional area of plain concrete, overlooking the impacts of internal reinforcement and concrete confined by stirrups. Two key stiffness properties, namely axial stiffness (AE) and bending stiffness (EI), are significant in analyzing multistorey reinforced concrete structural modeled as plane frames. By precisely determining the elastic modulus and geometric properties, the analysis can potentially become more accurate, leading to more economical designs. This study aims to examine the elastic modulus of the RC element, which has had limited study. It was Kulkarni et al. (2014) and Satya et al. (2016) that worked on the elastic modulus of RC; however; the authors did not transform the RC section. The gross moment of inertia was considered instead of the uncracked transformed moment of inertia. This study considered the transformed moment of inertia as an input variable. The planned laboratory studies entail applying bending stress to 100 × 150 × 1100 mm reinforced concrete beams with different reinforcing ratios and concrete compressive strengths.

2. MATERIALS AND METHOD

2.1. Material

The reinforced concrete beams (RCB) were produced with Portland limestone cement of 42.5 N grade, according to BS EN 197-1 (2011) and coarse and fine aggregates with specific gravities of 2.65 and 2.72, respectively. The concrete grades considered were M7.5, M10, M15, and M20. The concrete water to cement ratio for all mixes is 0.5. The beam of $100 \times 150 \times 1100$ mm was chosen based on the shear span to beam depth ratio of 2.55, as suggested by Biao & Yu-Fei (2018). According to EN 1992-1 (2004), the recommended minimum steel area is 0.13% of the effective sectional area, with a maximum of 0.4% of the gross crosssectional area. The beam samples were reinforced based on EN 1992-1 (2004). Table 1 provides the steel area for various concrete grades and beam geometry used in the experimental program.

2.2. Beam sample

A total of 36 reinforced concrete (RC) beams of size $100 \times 150 \times 1100$ mm were cast. The concrete beam

specimens were produced with different concrete grades and were categorized into four groups. The first group comprised beams with a concrete grade of 7.5 MPa and with varied reinforcement ratios of 0.43, 0.77, and 1.77, and were denoted as A-6T, A-8T, and A-12T, respectively, within the research framework as presented in Table 1. The second, third, and fourth group beams were produced with a concrete grade of 10, 15, and 20 MPa, respectively, and with varied reinforcement ratios as presented in Table 1. The first letter denotes the sample group (A, B, C, and D), while the second letter denotes tension reinforcement. The numbers (6, 8, 10, and 12) denote the diameter of the tension reinforcement. After casting, the beams were covered with polyethylene sheets and cured in a moist room at 20±2°C for 28 days until testing.

2.3. Test setup

Three concrete samples of 150 mm diameter x 300 mm height were cast and cured under identical conditions to the beams. On the day of the beam test, these concrete specimens were tested to determine compressive strength. The compressive strength from the three samples was computed according to BS EN 12390-3 (2009). The beam samples were tested on a 50-ton loading frame setup as a simple-supported beam with a one-third point load application, as shown in Figure 1. A dial gauge was positioned at the tension face of the beam, and steel rollers were also positioned at both ends to provide supports. The loading of the beams was done by means of a hydraulic jack and observed in a load cell. Readings were taken at each 1.0-ton increment, and the corresponding deflection was recorded on the dial gauge.

Regression analysis was conducted to develop an equation that can reasonably predict the elastic modulus of reinforced concrete beams with a significant level of 0.05.

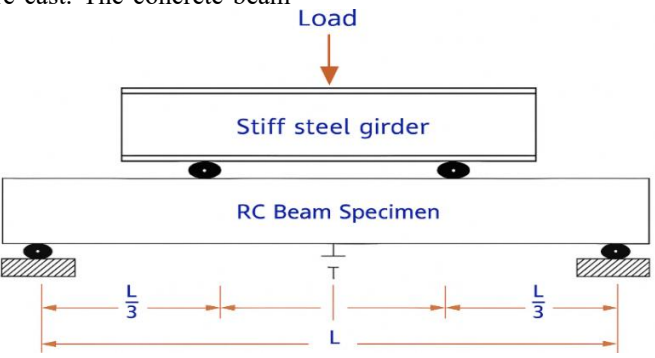


Figure 1. Schematic of test setup

Table 1. Beam geometry and reinforcement details

Sample ID	Beam geometry			Tension steel	Reinforcement	Concrete
	b(mm)	d(mm)	l(mm)	Area (mm²)	Ratio, ρ (%) Grade (MPa)	
A-6T	100	150	1100	56.56	0.43	7.5
A-8T	100	150	1100	100.54	0.77	7.5
A-12T	100	150	1100	226.22	1.77	7.5
B-6T	100	150	1100	56.56	0.43	10
B-8T	100	150	1100	100.54	0.77	10
B-12T	100	150	1100	226.22	1.77	10
C-6T	100	150	1100	56.56	0.43	15
C-8T	100	150	1100	100.54	0.77	15
C-10T	100	150	1100	157.10	1.2	15
C-12T	100	150	1100	226.22	1.77	15
D-6T	100	150	1100	56.56	0.43	20
D-8T	100	150	1100	100.54	0.77	20
D-10T	100	150	1100	157.10	1.2	20
D-12T	100	150	1100	226.22	1.77	20

2.4. Development of elastic modulus equations

The study made use of the elastic modulus equations (7) and (19) developed below as the key choice for determining the elastic modulus of RC concrete. These equations are considered vital in precisely calculating the elastic properties of RC. Figure 2 represents the experimental setup and the structural response. Equation (7) was developed based on the deflection expression as presented in Equation (1) (Buick & Graham, 2012).

From Figure 2(a) and Figure 2(d), the maximum deflection (δ) for the beam is expressed as:

$$\partial = \frac{23PL^3}{648EI} \tag{1}$$

where:

 P_{cr} is the critical load

L is the span length of the beam

E is the modulus of elasticity.

I is the moment of inertia.

From Figure 2(a) and Figure 2(b), the maximum bending moment (M) can be derived as:

$$M = \frac{PL}{3} \tag{2}$$

However, when considering a one-third point load application, the load Pcr is halved for one side of the

beam, leading to P=Pcr/2. Substituting this into Equation (2), the revised expression becomes

$$M = \frac{PL}{6} \tag{3}$$

Rewriting Equation (1), the modulus of elasticity E can be isolated as follows:

$$E = \frac{23PL^3}{648I\partial} \tag{4}$$

or

$$E = 0.0355 \,\mathrm{x} \, \frac{\mathrm{P}L^3}{12} \tag{5}$$

This equation allows the calculation of E, given the deflection (δ), moment of inertia (I), critical load (Pcr), and beam span (L).

Rewriting Equation (3) to express the cracking load P in terms of the other parameters, we get:

$$P = \frac{6M}{L} \tag{6}$$

Substituting P into Equation (4), we have:

$$E = \frac{0.213ML^2}{\partial I_{vm,tr}} \tag{7}$$

where:

 $M = M_{cr} = Cracked mement (kNm)$ $\partial = deflection at first crack (mm)$

 $I = I_{un,tr}$

= uncracked transformed moment of inertia

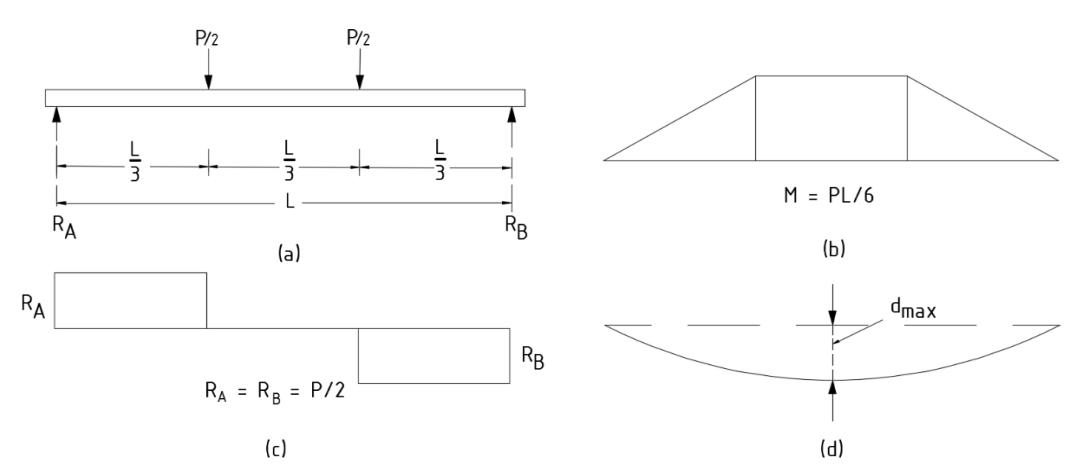


Figure 2. (a) Sample setup, (b), Moment diagram, (c) Shear Diagram, (d) deflection diagram

The uncracked transformed moment of inertia is determined using the parallel axis theorem, which accounts for the contribution of each material component to the overall section properties, incorporating the positional relationship of each component with respect to the neutral axis. Mathematically, it is defined as:

$$l_{un,tr} = \sum (I_i + A_i d_i^2) \tag{8}$$

I_i is moment of inertia of each component about its own centroidal axis.

A_i is Area of each component.

d_i is distance between the centroid of each component and the transformed section's neutral axis.

Before cracking, the beam's properties are determined based on the uncracked transformed section. The moment of inertia for the uncracked transformed section is given by:

$$l_{un,tr} = \frac{bh^3}{12} + bh\left(\bar{y}_t - \frac{h}{2}\right)^2 + (n-1)A_s(\bar{y}_t - d)^2$$
 (9)

The transformed centroid \bar{y}_t (from top of the section) is given as;

$$\bar{y}_t = \frac{\sum A_i \bar{y}_{t_i}}{\sum A_i} \tag{10}$$

The depth of transformed centroid \bar{y}_t (from top of the section) as presented in Figure 3(a), can be determine as;

$$\bar{y}_t = \frac{bh(\frac{h}{2}) + [(n-1)A_s](d)}{bh + (n-1)A_s}$$
(11)

The cracked moment can be computed as follow:

$$M_{cr} = \frac{f_t I_{un,tr}}{h - \bar{y}_t} \tag{12}$$

 $f_t = concrete tensile strength = 0.62\sqrt{f_{ck}}$

Considering the deformed beam shown in Figure 3(b)

let the length of the neutral axis be ff^i $\therefore ff^i = arc \ length = \theta R$ let's consider a very small layer with a thickness y adjacent to the neutral axis let the length be hh^I while the Radius of $hh^I = R + y$ $\therefore hh^i = arc \ length = \theta (R + y)$

Recall that strian,
$$\in = \frac{\text{change in length}}{\text{original}}$$

$$\in = \frac{(R+y)\theta - \theta R}{\theta R}$$

$$\in = \frac{(\theta R + \theta y) - \theta R}{\theta R}$$

$$\in = \frac{y}{R}$$
(13)

The elastic modulus can be defined as the ratio of stress to strain along the same axis within the elastic limit,

Hooks law can be applied as;

$$E = \frac{stress}{strain} = \frac{\sigma}{\epsilon}$$

$$E = \frac{\sigma}{\epsilon}$$
(14)

Substitute
$$\in = \frac{y}{R}$$
 and σ
= $\frac{M_{cr}}{Z}$ into Equation (14), we arrived at;

$$\frac{E}{R} = \frac{\sigma}{y} \tag{15}$$

Substitute
$$\sigma = \frac{M_{cr}}{Z}$$
, $Z = \frac{bd^2}{6}$ and y

$$=\frac{d}{2}$$
 into Equation (15), we arrived at;

$$E = \frac{RM_{cr}}{I_{un,tr}} \tag{16}$$

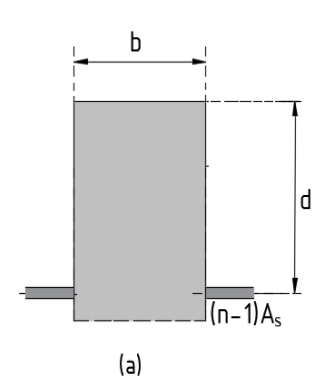
where: $R = Radius \ of \ the \ curvature \ (mm)$ Radius of the curvature (R) can be computed from Figure 3(c),

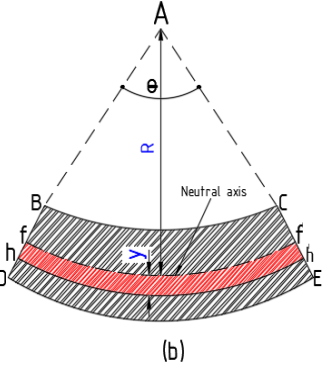
$$AE = R - \delta$$

$$EC = \frac{L}{2}$$

$$R^{2} = (R - \delta)^{2} + (\frac{L}{2})^{2}$$

$$R^2 = R^2 - 2R\delta + \delta^2 + \frac{L^2}{4} \tag{17}$$





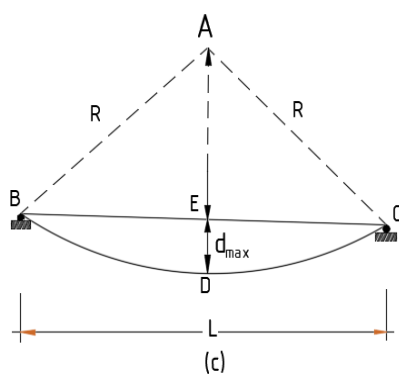


Figure 3. (a) Cracked transformed section, (b) and (c) Deformed beam Section

3. RESULTS AND DISCUSSION

3.1. Load-deflection behaviour

Figures 4 through 9 display the load-deflection curves for various concrete grades reinforcement ratios. Table 3 shows a transformed reinforcement portion with an equivalent area of concrete. The load against deflection curves for the M7.5, M10, M15, and M20 grade for the samples listed in Figures 4 to 9. The results presented in Figure 4 for beams with reinforcement ratios ρ of 0.43% and 0.77% for concrete grade M7.5. Figure 4 shows the load-deflection curves from the bending test for beams A-6T and A-8T with reinforcement ratios of 0.43% and 0.77%, respectively, using concrete grade M7.5. This trend conforms to typical

load-deflection responses observed in previous studies (Bhargava et al., 2006; Nakin et al., 2018).

Both curves exhibit an initial linear elastic response, indicating the uncracked behaviour of the reinforced concrete section. The higher initial stiffness of beam A-8T with $\rho = 0.77\%$ compared to beam A-6T with $\rho = 0.43\%$ can be attributed to its greater resistance to deformation owing to the larger amount of reinforcement (Kulkarni et al., 2014). The first visible deviation from linearity on both curves marks the initiation of cracking in the tension zone as the flexural stresses exceed the concrete tensile strength. Beam A-6T cracks at a load of 3.9 kN, with a corresponding deflection of 0.3 mm. Beam A-8T has a marginally higher first crack load of 4.24 kN and a deflection of 0.2 mm. This is consistent with

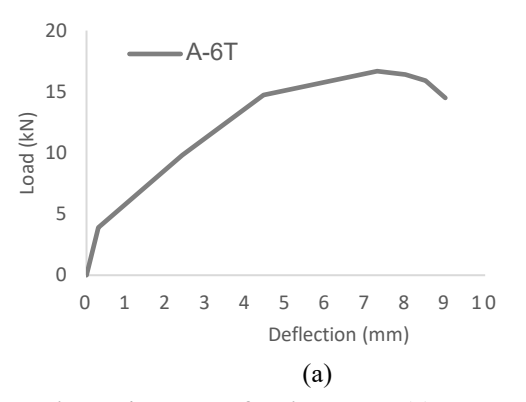
Simplifying equation (17), gives
$$R = \frac{4\delta^2 + L^2}{8\delta}$$
(18)

Equation (15) can be re-written as follows,
$$E = \frac{M_{cr}(4\delta^2 + L^2)}{\delta 8I_{un.tr}}$$
(19)

Equations (7) and (19) were used to compute the elastic modulus of reinforced concrete from bending test. Equation (19) links the beam's material properties to its mechanical response during a bending test. This formulation provides a practical way to determine the modulus of elasticity experimentally, using measurable parameters from the bending test. It is particularly significant in structural engineering as it accounts for the combined effects of material strength, geometry, and deflection, ensuring accurate characterization of reinforced concrete beams under load.

expectations, as the higher reinforcement ratio of A-8T delays cracking due to improved stress distribution. Post-cracking, both curves continue to increase approximately linearly but at a lower stiffness as the cracked, transformed section resists loading. Eventually, at high loads, localized failure develops, resulting in a descending portion of the curve. This confirms that after the formation of the first cracks, further loading does not induce additional cracks but causes widened crack openings in the tension zone instead. The slope of this cracked linear-elastic portion is steeper for A-8T, showing its improved composite action and enhanced stiffness. Yielding of reinforcement commences around loads of 12 kN and 18 kN for beams A-6T and A-8T, respectively, indicated by a change in curvature.. Within the loading range, no sign of brittle failure, such as aggregate interlock crushing, is observed, confirming the adequate

ductility of both sections. The test for beam A-6T was concluded upon reaching a maximum applied load of 16.68 kN, corresponding to a recorded deflection of 7.29 mm. Similarly, for beam A-8T, the peak load resistance of 30.41 kN was accompanied by a deflection of 6.05 mm, verifying its enhanced strength and serviceability due to its larger reinforcement content. Both responses match theoretical load-deflection behaviour, confirming the accuracy of the experimental setup and procedures adopted in this study. The loaddeflection curves presented validate the increase in cracking load, stiffness, flexural capacity, and ductility with a rising reinforcement ratio according to Kulkarni et al. (2014). This demonstrates the ability of the bending test to effectively evaluate flexural performance and capture the influence of reinforcement on load-deflection response.



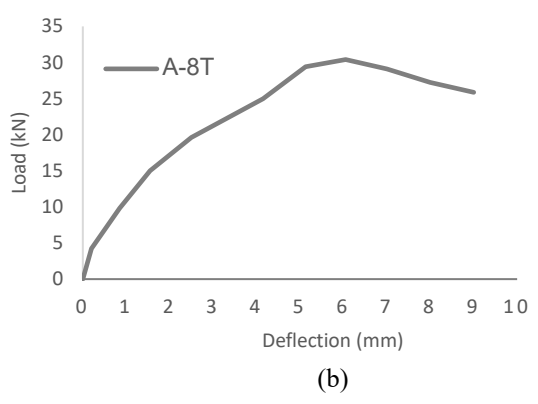


Figure 4. Load deflection curve (a) beam with $\rho = 0.43\%$ (M7.5), (b) beam with $\rho = 0.77\%$ (M7.5)

Figure 5 shows the load-deflection curves for beam A-12T and beam B-6T. For beam A-12T, the initial portion of the curve shows a linear relationship, indicating the beam's response was elastic up to the first crack load. The first crack was observed at a load of 5.1 kN, beyond which the curve became nonlinear as the load continued to increase and more cracks developed. This trend conforms to Yazdi et al. (2013). The cracking moment was calculated as 0.93 kNm from the first crack load and geometric properties using equation (4). After initial cracking, the slope of the curve gradually decreased, indicating that the stiffness of the beam was reducing. This could be attributed to the propagation of flexural cracks along the tension zone as the load increased further. At around 38 kN, the rate of deflection started increasing more rapidly. This represented the point where multiple cracks had coalesced across the beam's tension zone. Beyond this point, the response became highly nonlinear

until failure. For beam A-6T, the first crack was observed at a lower load of 3.9 kN compared to beam A-12T due to the lower concrete grade and reinforcement ratio. The cracking moment was computed as 0.82 kNm. Similar to beam A-12T, the initial linear elastic portion was followed by linear softening as cracks developed. However, the slope of the softening curve was more gradual compared to beam A-8T, indicating its stiffness reduced more gradually with loading. This was because the lower reinforcement ratio provided less crack control, allowing wider cracks to form. By comparing the two curves, it is evident that an increase in reinforcement ratio from 0.43% to 1.77% increased the cracking moment and load at first cracking substantially. This shows the reinforcing steel's influence in delaying crack initiation and development. Beam A-12T also exhibited a steeper drop in stiffness after initial cracking compared to A-6T due to better crack control from its higher

10 11

reinforcing ratio. These results validate the reinforcement ratio's significant effect on the flexural response and serviceability of RC beams. These load-deflection curves provide useful insights into the cracking behaviour and stiffness degradation mechanisms of RC beams with different concrete grades and reinforcement levels.

Increasing both properties enhances flexural strength and durability. This is consistent with findings from Satya et al. (2016) that demonstrated an increasing steel reinforcement ratio leads to a higher cracking load capacity due to enhanced composite action between steel and concrete.

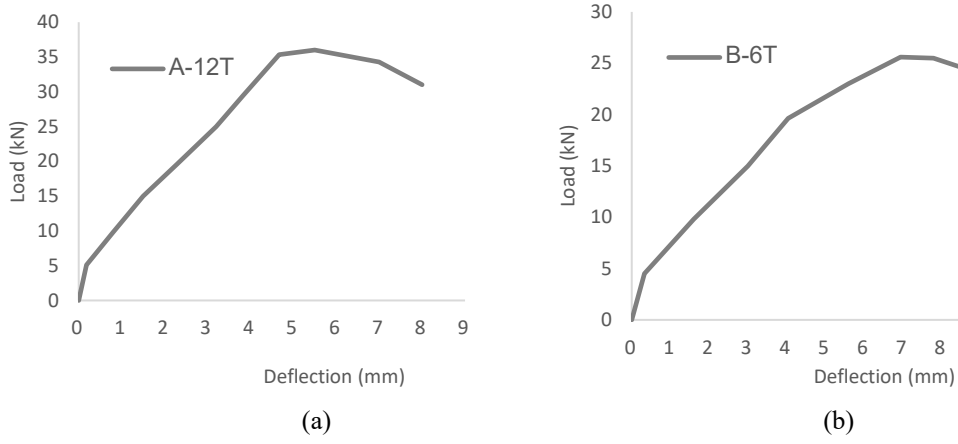


Figure 5. Load-deflection curve (a) A-12T; (b) B-6T

Figure 6 shows the load-deflection curves for beams B-8T and B-12T with reinforcement ratios of 0.77% and 1.77%, respectively, and a concrete grade of M10. From curve (a), it can be seen that beam B-8T with a reinforcement ratio of 0.77% exhibited an initial cracking load of approximately 4.8 kN, corresponding to a deflection of 0.25 mm. Beyond first cracking, the curve follows a descending trend with small fluctuations, indicating additional crack formations and propagations under increasing load. The maximum load carried by the beam was around 35 kN at a deflection of 11 mm. In comparison, beam B-12T with a higher reinforcement ratio of 1.77%, as shown in curve (b), displayed a higher initial cracking load of approximately 5.6 kN and a

lower corresponding deflection of 0.20 mm. This validates the concept that a higher reinforcement ratio improves stiffness by delaying the onset and widening of cracks (Kulkarni et al., 2014). This indicates that the higher steel content provided better crack resistance. Beyond first cracking, the load-deflection curve maintained a steadier descending trend compared to A-8T, showing that the increased reinforcement was more effective in controlling crack widths and hindering further crack propagation. The maximum load for B-12T was around 38 kN at a deflection of 5.4 mm, which is higher than B-8T, demonstrating improved structural performance with increased steel reinforcemen.

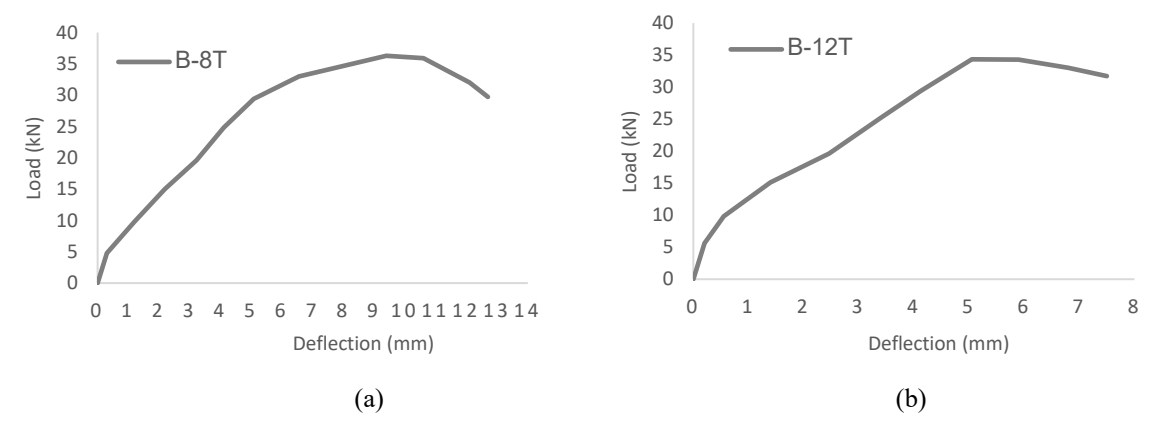
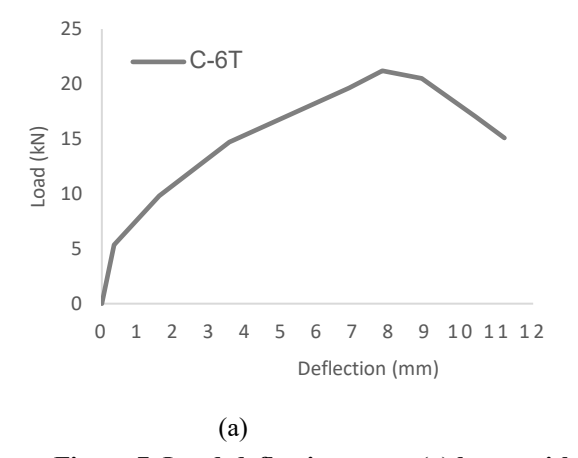


Figure 6. Load-deflection curve (a) beam with $\rho = 0.77\%$ (M10), (b) beam with $\rho = 1.77\%$ (M10)

Figure 7 presents the load-deflection behaviour for beams C-6T and C-8T with 0.43% and 0.77% reinforcement ratios, respectively, and a concrete grade of M15. Beam C-6T cracked initially at a load of around 5.3 kN, corresponding to a deflection of 0.24 mm, as shown in curve Figure 6(a). The initial parts of both the curves are linear and elastic in behavior up to the first cracking load. This behavior confirms that prior to cracking, the whole section is effective in resisting bending moment, as reported by Lee et al. (2015). After cracking, the loads fluctuated within a narrow band as deflections increased, reaching a maximum of 23 kN at 7.5 mm deflection. For beam C-8T with a higher steel ratio of 0.77%, as depicted in curve (b), the initial cracking load was higher at 5.67 kN but with a lower deflection of 0.22 mm in comparison. Beyond cracking, the load-carrying capacity degraded in a stable manner until reaching a maximum load of 45 kN at a deflection of 8 mm.

By comparing the curves in Figures 6 and 7, it can be observed that beams with a higher reinforcement ratio generally displayed higher cracking loads and strengths compared to those with a lower reinforcement ratio. Additionally, within the same reinforcement ratio, specimens with increased concrete grade exhibited improved initial crack resistance and structural response in terms of loadcarrying capacity and ductility. These trends emphasize the advantages of using stronger concrete and including sufficient reinforcing steel to improve the bending behavior and performance of RC beams. Thus, the load-deflection curves shown in Figure 7 are in good agreement with the findings reported in the studies by Jin and Li (2003), Yazdi et al. (2013), Lee et al. (2015), and Nakin et al. (2018) regarding the general behavior of reinforced concrete beams and influence reinforcement. This validates the results obtained in the current study.



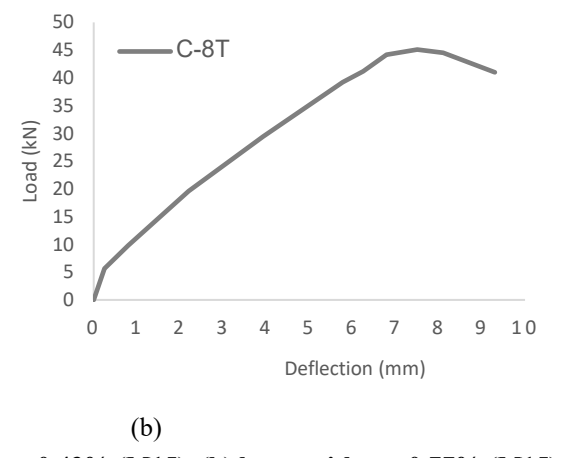


Figure 7. Load-deflection curve (a) beam with $\rho = 0.43\%$ (M15), (b) beam with $\rho = 0.77\%$ (M15)

Figure 8 shows the load-deflection curves for beams C-10T and C-12T with reinforcement ratios (p) of 1.2% and 1.77%, respectively, and a concrete grade of M15. It can be seen that the load-carrying capacity increased with the increase reinforcement ratio. Beam C-10T with $\rho = 1.2\%$ cracked at a load of around 6.1 kN with a corresponding deflection of 0.2 mm. Meanwhile, Beam C-12T with a higher reinforcement ratio of ρ = 1.77% cracked at a higher load of around 6.5 kN and a deflection of 0.19 mm. This indicates that the cracking moment and corresponding deflection decreased with the increase in reinforcement ratio

due to the stiffening effect of the reinforcement. This validates the findings of (Kulkarni et al., 2014). The initial stiff part of the curves also appeared steeper for beam C-12T, showing that it was stiffer prior to cracking compared to beam C-10T owing to its higher reinforcement ratio. After cracking, both curves continued increasing almost linearly up to the ultimate load. Beam C-12T achieved a higher ultimate load of around 60 kN compared to 50 kN for beam C-10T. This confirms that the load-carrying capacity increased with the reinforcement ratio due to the increased tensile strength provided by the reinforcement.

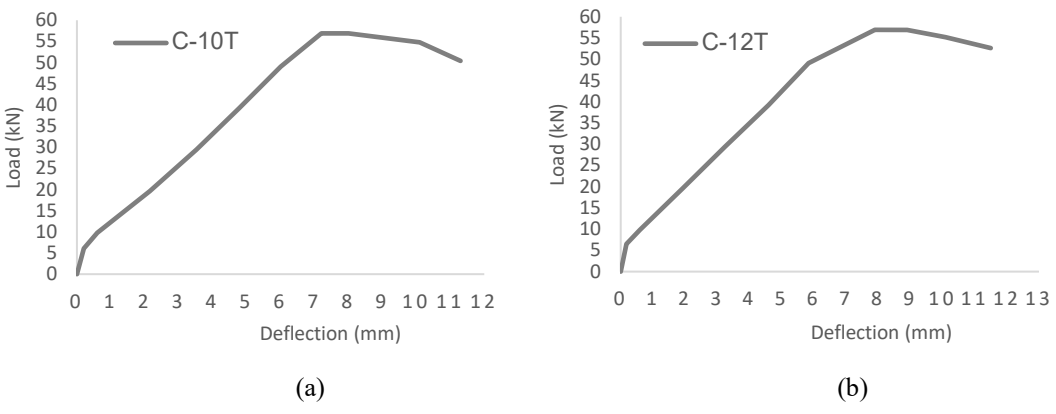


Figure 8. Load-deflection curve (a) beam with $\rho = 1.2\%$ (M15), (b) beam with $\rho = 1.77\%$ (M15)

Figure shows the load-deflection curves for beams D-6T and D-8T with ρ of 0.43% and 0.77%, respectively, and concrete grade M20. Similar to the M15-grade beams, it is evident that the loadcarrying capacity is enhanced with increasing reinforcement ratios. Beam D-6T cracked at 6.1 kN, while beam D-8T cracked at a higher load of 6.4 kN. The cracking deflection also reduced slightly from 0.24 mm to 0.22 mm. Both beams exhibited a linear increase in load versus deflection response until failure. Beam D-8T achieved an ultimate load of 50 kN compared to 20 kN for beam D-6T, indicating improved ductility and strength with increasing reinforcement. The uncracked stiffness increases with the addition of reinforcement because of the composite action between concrete and steel. As the reinforcement ratio increases from 0.43% to 0.77%, the uncracked stiffness is higher for the latter case (beam B-8T), as seen by the steeper initial slope. This validates the findings of Nakin et al. (2018) that flexural reinforcement enhances the uncracked bending resistance. The first crack moment (Mcr) is higher for the 0.77% reinforced beam. This is because the inclusion of steel induces confining pressure in concrete through dowel action, delaying crack initiation (Abdullah et al., 2023).

Figure 10 illustrates the load-deflection behavior of beams D-10T and D-12T, each constructed with a reinforcement ratio (ρ) of 1.2% and 1.77%,

respectively, and concrete grade M20. Beam D-10T experienced its first crack at an applied load of 5.8 kN and a corresponding deflection of 0.21 mm, while beam D-12T showed its first crack at a higher load of 7.2 kN with a slightly lower deflection of 0.19 mm. Both load-deflection curves exhibit an almost linear response up to the point of failure, indicative of elastic behavior in the uncracked phase, followed by the gradual development of plasticity. The ultimate load capacities for beams D-10T and D-12T were recorded as 50 kN and 55 kN, respectively, highlighting the significant enhancement in load-carrying capacity with an increase in steel reinforcement ratio.

The findings clearly demonstrate that higher reinforcement ratios improve both the cracking and ultimate load behavior of beams. For example, the beam with ρ =1.77%, as depicted in Figure 10(b), developed its first crack at a load of 7.2 kN and a deflection of 0.15 mm. This beam exhibited a higher cracking load and deflection compared to the beam with ρ =1.2%, owing to the increased moment capacity provided by the additional steel reinforcement. These observations align closely with the findings of Kulkarni et al. (2014), confirming that higher steel ratios enhance both stiffness and cracking resistance. This behavior is consistent across beams of M15 and M20 grade concrete.

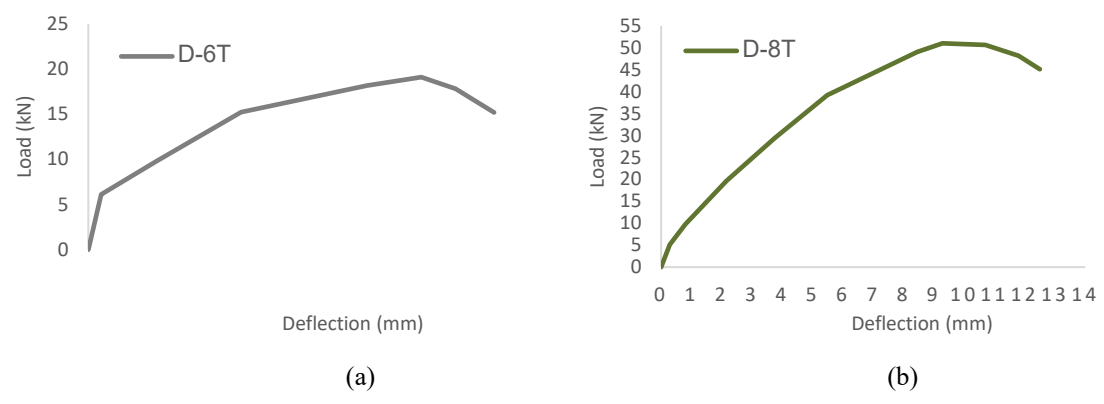


Figure 9. Load-deflection curve (a) beam with $\rho = 0.43\%$ (M20), (b) beam with $\rho = 0.77\%$ (M20)

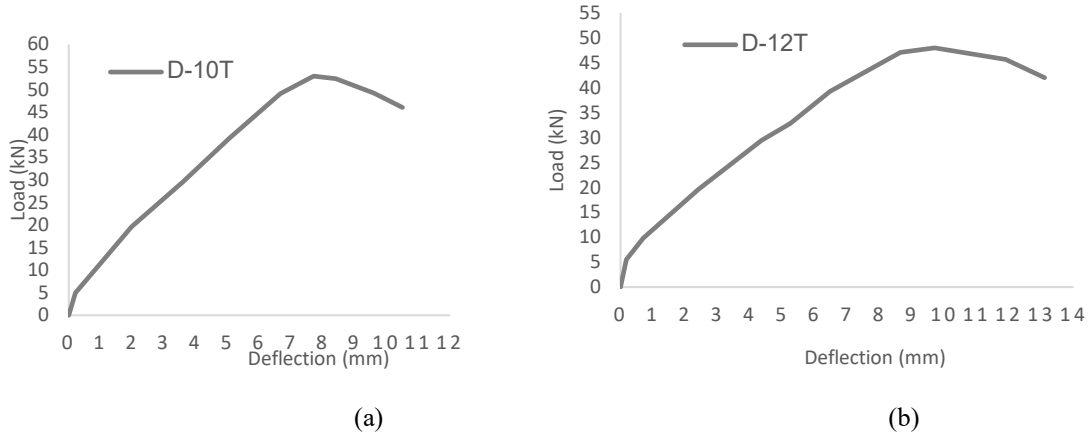


Figure 10. Load-deflection curve (a) beam with $\rho = 1.2\%$ (M20), (b) beam with $\rho = 1.77\%$ (M20)

3.2. Elastic modulus of reinforced concrete

The results of the elastic modulus of concrete and RC from the bending test are presented in Tables 3 and 4, respectively. The first crack load and the corresponding deflection were measured from the load-deflection curve presented in Table 2 and substituted into equations (7) and (19) for each beam type. The uncracked transformed moment of inertia was calculated using equation (9). By substituting the Mcr, L, δ and Iun, tr, the elastic modulus (E) of RC was evaluated as presented in Table 4. The elastic properties of plain concrete were determined based on ACI 318 (2014), as given in equation (20).

$$E_C = 4700\sqrt{f_{ck}} \tag{20}$$

Where:

 E_C is elastic properties of plain concrete (Mpa)

Table 2. Cracking moment and corresponding deflection

Sample	$M_{\rm C}$	Deflection	L	P _{Cr}
I.D	(kNm)	(mm)	(mm)	(kN)
A-6T	0.70	0.30	1100	3.9
A-8T	0.78	0.20	1100	4.24
A-12T	0.93	0.18	1100	5.1
B-6T	0.82	0.29	1100	4.5
B-8T	0.87	0.25	1100	4.8
B-12T	1.00	0.20	1100	5.6
C-6T	0.98	0.24	1100	5.35
C-8T	1.03	0.22	1100	5.67
C-10T	1.10	0.20	1100	6.1
C-12T	1.20	0.19	1100	6.5
D-6T	1.10	0.25	1100	6.1
D-8T	1.20	0.24	1100	6.4
D-10T	1.25	0.21	1100	6.8
D-12T	1.30	0.19	1100	7.2

The cracking load, Pcr, and the corresponding deflection, measured from the load-deflection response obtained from the experimental investigation, are summarized in Table 2. The cracking moment values were calculated using Equation 12 $(M_{cr} = \frac{f_t I_{un,tr}}{h - \bar{y}_t})$. The cracking moment was found to range from 0.70 kNm to 1.30 kNm for the tested beams. In general, the beams exhibited a trend of increasing cracking moment with increasing reinforcement ratio and concrete grade. Beams A-6T, A-8T, and A-12T made with M7.5 concrete showed cracking moments of 0.70 kNm, 0.78 kNm, and 0.93 kNm, respectively. This indicates that the cracking moment increased with the reinforcement ratio for the same concrete grade due to the increased tensile resistance provided by the steel. Similarly, beams B-6T to D-12T made with increasing concrete grades of M10, M15, and M20 also exhibited higher cracking moments with values ranging from 0.82 kNm to 1.30 kNm. The increase in concrete compressive strength positively influenced the tensile strength and thus resulted in higher cracking moments. The corresponding deflections at first cracking presented a decreasing trend with increasing reinforcement ratio and concrete grade. Beam A-6T with the lowest reinforcement ratio of 0.43% exhibited the highest deflection of 0.30mm, while beam A-12T with the highest reinforcement ratio of 1.77% for M7.5 concrete showed the lowest deflection of 0.18mm. This can be attributed to the increased stiffness of the section with a higher steel content, preventing large deflections. Similarly, the deflections decreased from 0.29mm to 0.19mm with an increase in concrete grade from M10 to M20 for the same reinforcement ratio. The higher the concrete grade, the greater its modulus of elasticity, resulting in reduced cracking deflections. These findings are supported by the studies of Kulkarni et al. (2014) and Satya et al. (2016), where they also reported increased first cracking load and corresponding deflection with increasing reinforcement ratio. This is attributed to the confinement effect provided by the reinforcement, which delays crack initiation. Confinement allows concrete to carry higher stresses before cracking by bridging across cracks (Nakin et al., 2018). Deformation capacity and ductility of concrete members are enhanced due to the confinement effect (Bhargava et al., 2006). The experimental results clearly demonstrate that increasing both the reinforcement ratio and concrete grade positively influences the cracking behaviour of RC beams. Higher reinforcement content and

concrete strength enhance the cracking moment capacity as well as reduce the deflection at the initiation of cracking. These trends are in good agreement with established structural behaviour and validate the test methodology adopted for the investigation. The data obtained provide insights into the cracking response of RC and establish a benchmark for further elastic modulus determination.

The results from Tables 3 and 4 provide valuable insights into the elastic modulus of reinforced concrete beams tested under bending. Table 3 shows the transformed steel portion calculated based on the modular ratio (n), which is the ratio of the elastic modulus of steel (Es) to that of concrete (Ec). This modular ratio allows transforming the steel reinforcement into an equivalent area of concrete, which has the same axial stiffness (AE). As can be seen in Table 3, the modular ratio (n) remains constant for each concrete grade since the elastic modulus of steel does not change. However, the elastic modulus of concrete (Ec) increases with the concrete's compressive strength, in line with code equation 20. For the M7.5-grade concrete, the EC is calculated at 12,871.5 MPa. This Ec value is then used to determine the modular ratio n, assuming a standard Es value of 200 GPa. Similarly, higher Ec values of 14,862.7 MPa, 18,203 MPa, and 21,019 MPa are obtained for the M10, M15, and M20 grade concretes, respectively. This transformed steel area concept allows for the analysis of the RC section using elastic beam theory. It accounts for the contribution of steel reinforcement towards the flexural and shear stiffness of the cracked, transformed RC section. Before cracking occurs, the transformed area is (n-1) times the actual steel area for both tension and compression reinforcement. This represents the additional stiffness provided by the steel bars to the surrounding concrete.

Table 4 presents the results for the percentage of steel reinforcement, the uncracked transformed moment of inertia ($I_{un, tr}$), and the corresponding elastic modulus (E) of the reinforced concrete as determined using Equation (7) and (19). The elastic moduli derived from Equations (7) and (19) are denoted as E_7 and E_{19} , respectively. The elastic modulus (E) of the reinforced concrete is taken as the average of the values calculated from Equations (7) and (19). It can be seen that as the percentage of steel increases for a given concrete grade, the uncracked transformed moment of inertia ($I_{un, tr}$) also increases. This is because a higher steel ratio results in a larger transformed steel area, thereby enhancing

the second moment of area and the stiffness of the section. Correspondingly, the elastic modulus (E) of RC increases with a rising steel percentage. For example, in the M7.5 concrete beams, E increases from 25.7 GPa for 0.43% steel to 30.9 GPa for 1.77% steel. This confirms that steel reinforcement positively influences the flexural rigidity and stiffness of RC elements. A stiffer section experiences lower deflections under the same loading. demonstrating improved performance. An important observation is that E increases significantly with concrete grade, even when the steel percentage is kept constant. Taking the 0.43% steel beams as an example, E rises from 25.7 GPa at M7.5 grade to 31.1 GPa at M20 grade. This indicates that while steel reinforcement enhances E, the primary factor governing E is the compressive strength (and associated stiffness

properties) of concrete. Higher-strength concrete exhibits superior load-carrying capacity and deforms less under load due to its dense microstructure. These results correlate well with the research carried out by Kulkarni et al. (2014) and Satya et al. (2016).

The results effectively validate the methodology adopted to determine the elastic modulus (E) of RC. Both Tables 3 and 4 collectively demonstrate that E is influenced positively by the concrete grade as well as the reinforcement ratio. The observations are useful in accurately representing the composite behaviour of reinforced concrete in numerical models and design codes. The elastic modulus is a vital material property governing stress-strain response and dimensional changes in RC elements subjected to working loads.

Table 3. Transformed steel portion with an equivalent area of concrete

Sample ID	Concrete grade (MPa)	Ec (MPa)	Es (MPa)	$n = {^E S}/_{E_C}$	As (mm ²)	(n-1) As (mm ²)
A-6T	7.5	12871.5	200000.0	15.5	56.6	822
A-8T	7.5	12871.5	200000.0	15.5	100.5	1462
A-12T	7.5	12871.5	200000.0	15.5	226.2	3289
B-6T	10	14862.7	200000.0	13.5	56.6	705
B-8T	10	14862.7	200000.0	13.5	100.5	1252
B-12T	10	14862.7	200000.0	13.5	226.2	2818
C-6T	15	18203.0	200000.0	11.0	56.6	565
C-8T	15	18203.0	200000.0	11.0	100.5	1004
C-10T	15	18203.0	200000.0	11.0	157.1	1569
C-12T	15	18203.0	200000.0	11.0	226.2	2259
D-6T	20	21019.0	200000.0	9.5	56.6	482
D-8T	20	21019.0	200000.0	9.5	100.5	856
D-10T	20	21019.0	200000.0	9.5	157.1	1338
D-12T	20	21019.0	200000.0	9.5	226.2	1926

Table 4. Percentage of steel, cracked transformed moment of inertial and corresponding E value of RC

Sample ID	I _{un, tr} (mm ⁴)	Concrete grade (MPa)	ρ (%)	E ₇ (MPa)	E ₁₉ ((MPa)	(E7+E19)/2
A-6T	30569664	g ()	0.43	19672	11545	15,609
A-8T	32153961	7.5	0.77	31260	18345	24,803
A-12T	35990660		1.77	36999	21713	29,356
B-6T	30235316		0.43	24103	14145	19,124
B-8T	31621509	10	0.77	28364	16645	22,505
B-12T	35042499		1.77	36774	21581	29,178
C-6T	29832160	15	0.43	35277	20703	27,990
C-8T	30971866		0.77	38959	22863	30,911
C-10T	32266925		1.2	43931	25781	34,856
C-12T	33640615		1.77	48387	28396	38,392
D-6T	29588370		0.43	38326	22492	30,409
D-8T	30574924	20	0.77	42147	24734	33,441
D-10T	31706435		1.2	48385	28395	38,390
D-12T	32920190		1.77	53566	31436	42,501

The modulus of elasticity represents a material's stiffness, defined by the relationship between stress and strain in the elastic range. In reinforced concrete (RC) structures, deflection under a known load is directly linked to the flexural stiffness of the beam or slab, allowing the modulus of elasticity to be calculated. At the cracking position, deflection at the cracking load is particularly important as it captures the material's stiffness during the transition from uncracked to cracked behavior. This modulus at cracking is critical for refining serviceability predictions and enhancing the accuracy of nonlinear analyses.

Multiple regression analysis was conducted on the elastic modulus of the RC values presented in Table 4. Equation (21) is derived from experimental data through multiple regression analysis, making it suitable for predicting the elastic modulus E of reinforced concrete beams with varying f_{ck} and ρ . The equation contains ten terms, with varying powers and interaction effects of f_{ck} and ρ . These account for nonlinear and combined influences on the elastic modulus E, making the equation capable of capturing complex relationships.

The constant term (35740) provides the base elastic modulus value when both f_{ck} and ρ are zero. Linear terms $(-8837f_{ck} + 34797\rho)$ reflect direct proportional or inverse relationships. Quadratic terms $(966f_{ck}^2 + 4867\rho^2)$ capture curvature in the relationship, suggesting diminishing or increasing returns. Cubic terms $(-26f_{ck}^3 - 5270\rho^3)$ model extreme nonlinearity, particularly relevant at high values of fck or ρ . Interaction terms (3339 $f_{ck}\rho + 71\rho f_{ck}^2 + 587f_{ck}\rho^2$) account for combined effects, where the impact of one variable depends on the level of the other.

The units in Equation (21) are defined as follows: Elastic Modulus (E): Typically measured in megapascals (MPa). Concrete Grade (fck): Characteristic compressive strength, expressed in MPa. Reinforcement Ratio (ρ): Represented as a percentage but utilized in its decimal form within the equation (e.g., 2% is expressed as 0.02).

The strength of Equation (21) is presented in Figure 11. Figure 11(a) presents a comparison between the elastic modulus (E) values predicted using Equation (21) and those determined experimentally through flexural tests. The plot indicates a reasonably good correlation between the predicted and actual E for all concrete grades. This validates the accuracy of the methodology adopted for experimentally

determining E. It also establishes the reliability of using code-predicted E values for preliminary design calculations. As seen in the figure, most data points are clustered around the parity line, representing identical predicted and actual E. This suggests a close match between the two sets of values. Only a few outlier points exhibit marginal deviations, possibly arising from minor test inaccuracies. On the whole, the results corroborate the ability of prediction models prescribed in codes to realistically forecast the elastic behaviour of reinforced concrete. It can be observed that the experimental E values predominantly exceed the predictions at higher concrete compressive strengths beyond 15 MPa. The observed discrepancies can be attributed to the amplified influence of the reinforcement ratio (ρ) and higher-order terms (e.g., secondand third-order), which increasingly significant at elevated concrete strengths. Even marginal inaccuracies in the estimated coefficients or interaction terms within the predictive model can propagate into more pronounced errors. Furthermore, high-strength concrete exhibits unique microstructural properties, including reduced porosity and denser aggregatematrix bonding, which may deviate from the idealized assumptions underlying the regression model, thereby contributing to the variations. This positive differential can be attributed to the multiaxial stress states generated in confined concrete cylinders during compression testing. In contrast, beam bending induces uniaxial stresses, yielding a marginally lower modulus. Additionally, factors like aggregate packing and interfacial transition zones are better accounted for through test data versus code assumptions. An important implication of this study is that code-prescribed modulus relationships can reliably estimate E for initial sizing and analysis of structural elements. This considerably simplifies design workflows since repeated, complex experimentation is avoided. At the same time, closer conformity between actual and predicted responses lends confidence in applying analytical or numerical models validated using codes. An accurate representation of E helps to evaluate deflections, stresses, and load distributions more precisely. The coefficient of regression was observed to be 0.9982, indicating an approximately 99.8% predictive capability as evidently shown in

Figure 11a. The equation (21) in terms of percentage of reinforcement and concrete grade can be considered making predictions about the elastic

modulus of RC at given levels of percentage of reinforcement and concrete grade.

$$E = 35740 - 8837f_{ck} + 34797\rho - 3339f_{ck}\rho + 966f_{ck}^{2} + 4867\rho^{2} + 71\rho f_{ck}^{2} + 587f_{ck}\rho^{2} - 26f_{ck}^{3} - 5270\rho^{3}$$
(21)

Where;

$$\rho = Reinforcement \ ratio \ (\%)$$
 $f_{ck} = Concrete \ grade \ (MPa)$

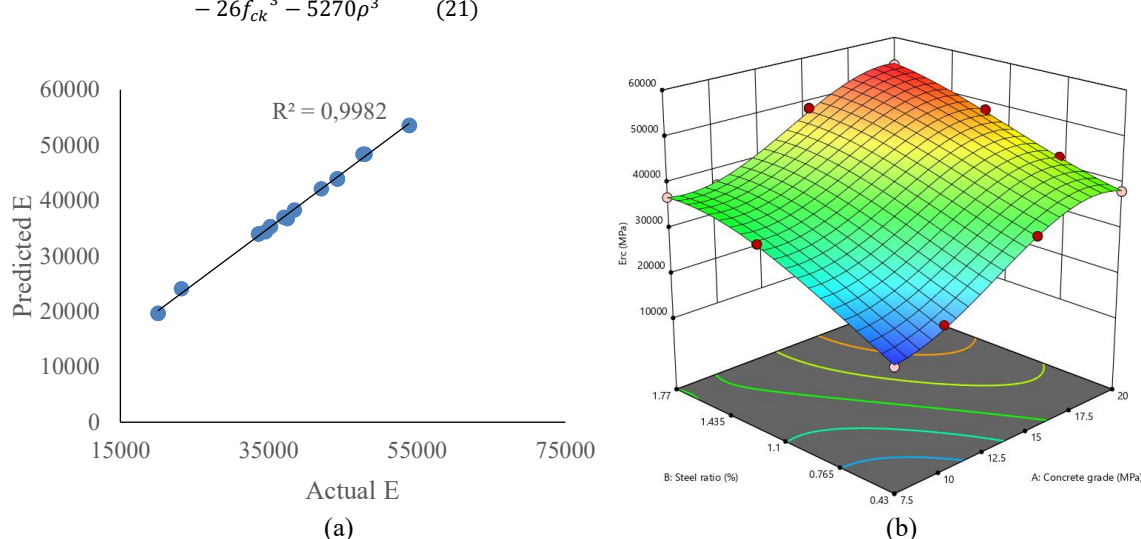


Figure 11. (a) Predicted - Actual elastic modulus; (b) Three-dimensional surface of the elastic modulus of RC model terms relative to reinforcement ratio and concrete grade

The systematic evaluation presented herein verifies the suitability of using code-based estimations to represent the elastic behaviour of reinforced concrete. Marginal variances are statistically insignificant. The findings endorse codes as a trusted design tool while highlighting the need for periodic validation against lab-derived data. This balanced approach achieves an optimal balance of economy, rationality, and safety in RC structure analysis and sizing.

Figure 11b exhibits the relationship between the key parameters governing the elastic modulus (E) of reinforced concrete through a three-dimensional surface model. The parameters considered are concrete compressive strength (f_c) reinforcement percentage (p), and the resulting E values. The positive sloping surface indicates that E increases simultaneously with rising f_c and ρ . Higher concrete strengths directly augment the intrinsic stiffness properties. Greater steel ratios, on the other hand, enhance the composite section's resistance to deformation via reinforcement confinement effects. This justifies the code specifications linking E to both materials' contributions. Notably, the effect of reinforcement on E is more prominent at lower fc levels. Its influence diminishes as the strength of concrete increases significantly. This implies that concrete quality assumes primacy over steel content

in dictating RC modulus. However, reinforcement still plays an important supportive role even when concrete is highly reinforced. The model reveals that the deviations between predicted and measured E, observed in some data points, are systematic rather than arbitrary. This lends credence to the developed relationship as a realistic representation of actual RC behaviour. Marginal non-linearity is also modelled appropriately instead of idealizing the response. The continuous graduated variation portrayed endorses the use of such analytical formulations for pre-construction design simulation and sensitivity Approximating E in a mathematically defined form improves reliability versus site-specific testing. It also aids in the life-cycle performance assessment of aged structures.

Figure 11b presents a useful visualization of test results. The 3D surface fitting technique establishes that experimental observations comply with theoretically expected trends. This finding substantiates the ability to characterize numerically the reinforced concrete elastic modulus based on material properties. It advocates computational modelling as a robust complement to codes.

The elastic modulus of RC with increasing reinforcement ratio and concrete grade is presented in Figure 11b. It is evident that the elastic modulus

of reinforced concrete (RC) exhibits a parabolic growth with increasing concrete grade, at a constant reinforcement ratio. Similarly, at a consistent concrete grade, the elastic modulus of RC follows a parabolic increase with an increasing reinforcement ratio. This observation highlights the relationship between concrete grade, reinforcement ratio, and the resultant elastic modulus of RC.

4. CONCLUSION

This research provides a comprehensive evaluation of the elastic modulus of RC with varying reinforcement ratios and different grades of concrete. As well, an in-depth database of elastic modulus results from the developed equation is used to evaluate the accuracy of the experimental elastic modulus results. From the investigation, the following conclusions are drawn:

The study revealed that as the concrete grade increases, so does the modulus of elasticity of the RC; however, this leads to a reduction in the modular ratio. This agrees with the established understanding that elastic modulus correlates positively with concrete compressive strength. As cement hydration advances with increasing strength, the concrete microstructure becomes denser, resulting in higher stiffness;

REFERENCES

- Abdullah, A., Sivakumar, K. G., & Abhishek, K. (2022). Elastic modulus of self-compacting fibre reinforced concrete: Experimental approach and multi-scale simulation. Case Studies in Construction Materials, 18, 1-14.
- American Concrete Institute. (2014). *Building code* requirements for structural concrete (ACI 318R-14). Farmington Hills, MI: Author.
- Aïtein, P. -C., & Mehta, P. K. (1990). Effect of coarse aggregate characteristics on mechanical properties of high-strength concrete. *ACI Materials Journal*, 87(2), 103–107.
- Alsalman, A., Dang, C. N., & Micah, W. H. (2019). Mixture-proportioning of economical UHPC mixtures. *J. Build. Eng.*, 27(2020), 100970, https://doi.org/10.1016/j.jobe.2019.100970
- Baalbaki, W., Benmokrane, B., Chaallal, O., & Aïtcin, P.C. (1991). Influence of coarse aggregate on elastic properties of high-performance concrete. ACI Materials Journal, 88(5), 499-503.
- Bae, B. I., Choi, H. K., Lee, B. S., & Bang, C. H. (2016). Compressive behavior and mechanical characteristics and their application to stress strain relationship of steel fiber-reinforced reactive powder

- At a consistent concrete grade, the elastic modulus of RC follows a parabolic increase with an increasing reinforcement ratio. This can be attributed to the confinement effect provided by steel reinforcement, which enhances the load-carrying capacity of the surrounding concrete. Additionally, incorporating more steel into the section using a larger transformed area in the analysis contributes to the overall stiffness. This observation highlights the relationship between concrete grade, reinforcement ratio, and the resulting elastic modulus of RC.
- The development of Equations 7 and 19 to determine the elastic modulus of RC based on flexural test parameters such as deflection, cracking moment and transformed sectional properties provides a more refined approach over codespecified relations. This is because the test setup considers the actual composite action between concrete and steel under service loads. And;
- When calculating the elastic modulus of reinforced concrete, it's imperative to used uncracked transformed reinforced concrete moments of inertia into the analysis for precise results.

CONFLICT OF INTEREST

The authors declare no conflicts of interest.

- concrete. Advances in Materials Science and Engineering, 2016, 1-11.
- Bhargava, P., Sharma, U. K., & Kaushik, S. K. (2006). Compressive stress-strain behavior of small-scale steel fibre reinforced high strength concrete cylinders. *Journal of Advanced Concrete Technology*, 4(1), 109-121.
- Biao, H., & Yu-Fei, W. (2018). Effect of shear span-to-depth ratio on shear strength components of RC beams. *Engineering Structures*, *168*, 770–78.
- BS EN 12390-3. (2009). Testing hardened concrete. Compressive strength of test specimens.
- Buick, D. & Graham, W. O. (2012). Steel designers' manual (7th ed.). The Steel Construction Institute.
- Choi, B. S., Oh, B. H., & Scanlon, A. (2002). Probabilistic assessment of ACI 318 minimum thickness requirements for one-way members. *ACI Structural Journal*, 99(3), 344–351.
- Christensen, R. M. & Lo, K. H, (2002). Solutions for effective shear properties in three phase sphere and cylinder models. *Journal of the Mechanics and Physics of Solids*, *27*(I4), 315-330.

- Chu, H. Y. L., Gao, J. J., Qin, J. Y., Jiang, J. Y., Jiang, & D. Q. W. (2022). Mechanical properties and microstructure of ultra-high-performance concrete with high elastic modulus. *Construct. Build. Mater*, 335.
- BS EN 197-1: (2011). Cement. Part 1: Composition, specifications and conformity criteria for common cements. London: BSI Standards Publication.
- Gutierrez, P. A., & Canovas, M. F. (1995). The modulus of elasticity of high-performance concrete. *Materials and Structures*, 28(10), 559-568.
- James, K. W., & James, G. M. (2012). Reinforced concrete mechanics and design (6th ed.). Library of Congress Cataloging-in-Publication Data.
- Jin, X., & Li, Z. (2003). Effects of mineral admixture on properties of young concrete. *Journal of Materials in Civil Engineering*, ASCE, 15(5) 435-442.
- Krystian, J., & Stefania, G. (2015). The influence of concrete composition on Young's modulus. Peerreview under responsibility of organizing committee of the 7th Scientific-Technical Conference Material Problems in Civil Engineering, Procedia Engineering 108, 584 591.
- Kulkarni, S. K. Shiyekar, M. R. Shiyekar S. M. (2014). Elastic properties of RCC under flexural loading-experimental and analytical approach. *Indian Academy of Sciences Sadhana*, 39(3), 677–697.
- Lee, B. J., Kee, S. H., Oh, T., & Kim, Y. Y. (2015). Effect of cylinder size on the modulus of elasticity

- and compressive strength of concrete from static and dynamic tests. *Advances in Materials Science and Engineering*, 1-12.
- Nakin, S., Salam, W., & Ahmed, A. (2018). Evaluation of elastic modulus of fiber-reinforced concrete. ACI Materials Journal, 115(2), 239 249.
- Peter, S., & Shuaib, A., (2000). Effect of transition zone on the elastic behavior of cement-based composites. *Cement and Concrete Research*, 25(1), 165-176.
- Richard, M. C. (2002). A critical evaluation for a class of micro-mechanics models. *Journal of the Mechanics and Physics of Solids*, 38(3), 379-404.
- Satya, P., Mohd, K. K., Imran, A. & Rajiv, B. (2016). Study of modulus of elasticity of RC beam under flexural loading using ANSYS. *International Journal of Scientific & Engineering Research*, 7(3), 1335-1344.
- Yang, C. C. A. (1998). Effect of the transition zone on the elastic moduli of mortar. *Cement and Concrete Research*, 28(5), 727-736.
- Yazdi, J. S., Kalantary, F., & Yazdi, H. S. (2013). Prediction of elastic modulus of concrete using support vector committee method. *Journal of Materials in Civil Engineering*, 25(1), 9-20. https://doi.org/10.1061/(ASCE)MT.1943-5533.0000507